Remote compositional analysis of lunar olivine-rich lithologies with Moon Mineralogy Mapper (M^3) spectra

Peter J. Isaacson,[1] Carle M. Pieters,[1] Sebastien Besse,[2] Roger N. Clark,[3] James W. Head,[1] Rachel L. Klima,[4] John F. Mustard,[1] Noah E. Petro,[5] Matthew I. Staid,[6] Jessica M. Sunshine,[2] Lawrence A. Taylor,[7] Kevin G. Thaisen,[7] and Stefanie Tompkins[8]

Received 31 August 2010; revised 6 January 2011; accepted 18 January 2011; published 26 April 2011.

[1] A systematic approach for deconvolving remotely sensed lunar olivine-rich visible to near-infrared (VNIR) reflectance spectra with the Modified Gaussian Model (MGM) is evaluated with Chandrayaan-1 Moon Mineralogy Mapper (M^3) spectra. Whereas earlier studies of laboratory reflectance spectra focused only on complications due to chromite inclusions in lunar olivines, we develop a systematic approach for addressing (through continuum removal) the prominent continuum slopes common to remotely sensed reflectance spectra of planetary surfaces. We have validated our continuum removal on a suite of laboratory reflectance spectra. Suites of olivine-dominated reflectance spectra from a small crater near Mare Moscoviense, the Copernicus central peak, Aristarchus, and the crater Marius in the Marius Hills were analyzed. Spectral diversity was detected in visual evaluation of the spectra and was quantified using the MGM. The MGM-derived band positions are used to estimate the olivine's composition in a relative sense. Spectra of olivines from Moscoviense exhibit diversity in their absorption features, and this diversity suggests some variation in olivine Fe/Mg content. Olivines from Copernicus are observed to be spectrally homogeneous and thus are predicted to be more compositionally homogeneous than those at Moscoviense but are of broadly similar composition to the Moscoviense olivines. Olivines from Aristarchus and Marius exhibit clear spectral differences from those at Moscoviense and Copernicus but also exhibit features that suggest contributions from other phases. If the various precautions discussed here are weighed carefully, the methods presented here can be used to make general predictions of absolute olivine composition (Fe/Mg content).

Citation: Isaacson, P. J., et al. (2011), Remote compositional analysis of lunar olivine-rich lithologies with Moon Mineralogy Mapper (M^3) spectra, *J. Geophys. Res.*, *116*, E00G11, doi:10.1029/2010JE003731.

1. Introduction

[2] The mineralogy and mineral composition of planetary samples contain a rich record of the thermal and chemical evolution of the planetary body. The processes responsible for the cooling of planetary bodies include magma ocean formation and solidification, differentiation (density stratification) and overturn, large-scale convection, and volcanic activity. These processes all produce distinct signatures in the mineral assemblages and compositions produced across a range of depths and across the body's surface. While the record can be complex, the composition and mineralogy of planetary samples represent one of the most powerful tools available for unraveling the geologic history of a planetary body. While returned samples are the most powerful tool for evaluating planetary composition and mineralogy, remote sensing, such as with orbital visible to near-infrared (VNIR) reflectance spectroscopy, offers a number of advantages. These advantages include global coverage (if conducted from orbit) and the ability to analyze composition without returned samples, although such remote measurements are greatly strengthened by the context and ground truth provided by returned samples [e.g., *Pieters*, 1999; *Taylor et al.*, 2001, 2010].

[3] Olivine in particular is a useful mineral with which to evaluate the geologic evolution of igneous planetary bodies such as the Moon. Olivine is typically one of the first minerals to crystallize from a mafic magma, and its composition is indicative of the composition and degree of

[1]Department of Geological Sciences, Brown University, Providence, Rhode Island, USA.
[2]Astronomy Department, University of Maryland, College Park, Maryland, USA.
[3]U.S. Geological Survey, Denver, Colorado, USA.
[4]Johns Hopkins University Applied Physics Laboratory, Laurel, Maryland, USA.
[5]NASA Goddard Space Flight Center, Greenbelt, Maryland, USA.
[6]Planetary Science Institute, Tucson, Arizona, USA.
[7]Planetary Geosciences Institute, University of Tennessee, Knoxville, Tennessee, USA.
[8]Defense Advanced Research Projects Agency, Arlington, Virginia, USA.

Copyright 2011 by the American Geophysical Union.
0148-0227/11/2010JE003731

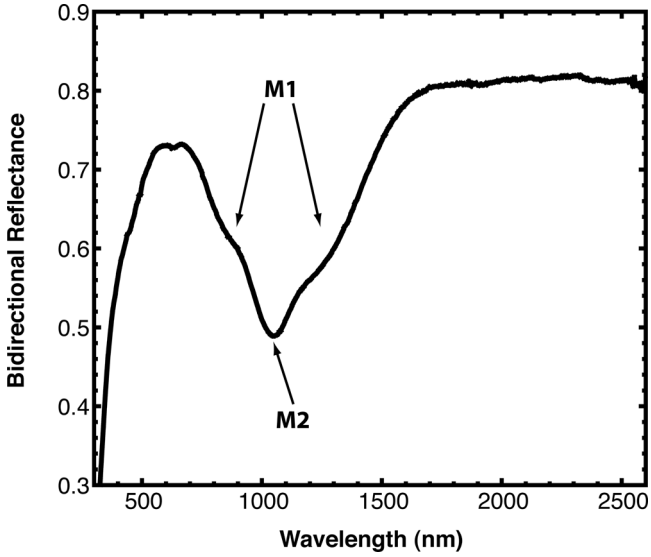

Figure 1. Bidirectional reflectance spectrum of San Carlos olivine (~Fo_{90}). The component absorptions that comprise the composite olivine 1000 nm absorption feature are labeled with the Fe^{2+}-bearing site responsible for the component absorption. Note the bright, featureless nature of the spectrum beyond ~1500 nm.

evolution of the source region in the case of a primary magma [*Basaltic Volcanism Study Project* (*BVSP*), 1981]. Recent results suggest that olivine is exposed largely in and around the rims of large lunar impact basins [*Yamamoto et al.*, 2010]. Such regions should represent some of the deepest materials excavated by the basin-forming impact. *Yamamoto et al.* [2010] argued that these olivine detections may represent exposures of the lunar mantle, but could also represent differentiated plutons resulting from secondary magmatic intrusions into the lunar crust. *Yamamoto et al.* [2010] favor the mantle source model as the more probable interpretation, based primarily on an apparent lack of plagioclase association with the olivine exposures. However, many of the detections are associated with exposures of "pure anorthosite" reported by *Ohtake et al.* [2009], and plagioclase is difficult to detect in the near-infrared when mixed with absorbing mafic minerals like pyroxene and olivine. While the detection of the olivine signature is critical, the composition of those olivines is an important additional clue to the olivine's source and history, as mantle olivines would be expected to be quite Mg-rich.

[4] Generally, for primary magmas, forsteritic (high Mg # (molar Mg/Mg+Fe)) olivine is indicative of a primitive source, and more fayalitic (low Mg #) olivine is indicative of a more evolved source [*BVSP*, 1981]. Lunar samples contain olivine of diverse compositions, from very Mg-rich (~Fo_{90}) in Mg suite rocks to more Fe-rich in basalts; olivines in basalts that are sufficiently abundant (>1–2 modal %) to be detectable through remote VNIR reflectance spectroscopy generally range from <Fo_{80} to ~Fo_{50} [e.g., *Papike et al.*, 1998]. Additionally, olivine has a distinctive signature in VNIR reflectance spectra, and this signature is compositionally dependent, meaning that remotely sensed VNIR reflectance spectra are sensitive to both the presence and composition of olivine on planetary surfaces [*Burns*, 1970; *King and Ridley*, 1987; *Sunshine and Pieters*, 1998; *Dyar et al.*, 2009]. Typical olivine spectra have a broad, composite absorption feature centered near 1050 nm. These absorptions are caused by electronic transitions in Fe^{2+} ions located in distorted octahedral crystallographic sites. The central absorption is caused by Fe^{2+} in the M2 site, while the two exterior absorptions are caused by Fe^{2+} in the M1 site [*Burns*, 1970; *Burns et al.*, 1972; *Burns*, 1974, 1993]. An example olivine spectrum is plotted in Figure 1, which shows the spectrum of San Carlos olivine (~Fo_{90}), a common laboratory standard due to its composition and relative purity. The three component absorptions that produce the composite absorption feature are labeled with the Fe^{2+}-bearing crystallographic site responsible for the component absorption.

[5] The properties of the three component absorptions are a function of the olivine's Mg #, and shift in regular, well-characterized ways with changing Mg # [*Sunshine and Pieters*, 1998]. When olivine spectra are deconvolved with quantitative techniques such as the Modified Gaussian Model (MGM), the MGM-derived band parameters of the individual component absorptions can be used to estimate the olivine's composition [*Sunshine et al.*, 1990; *Sunshine and Pieters*, 1998]. As demonstrated by previous work, these MGM-derived parameters can be applied to solve for olivine composition as a function of band position [*Sunshine and Pieters*, 1998; *Isaacson and Pieters*, 2010]. The relative strengths, and to a lesser extent, widths of the three component absorptions also shift with changing olivine Mg #, although this trend is less useful for compositional analysis.

[6] Compositional analysis of lunar olivines with VNIR reflectance spectroscopy is complicated by the presence of inclusions of Cr-spinel (largely chromite), which causes absorptions beyond ~1600 nm [*Cloutis et al.*, 2004; *Isaacson and Pieters*, 2010]. Inclusion-free olivine spectra are bright and featureless across this wavelength region, a property which was used to define a standard approach to deconvolutions of olivine spectra [*Sunshine and Pieters*, 1998]. The absorptions due to Cr-spinel inclusions, common in lunar olivines, cause the results of MGM deconvolutions of lunar olivine spectra to be inconsistent with deconvolutions of terrestrial olivine spectra of similar composition [*Papike et al.*, 1998; *Isaacson and Pieters*, 2010]. Because the terrestrial olivine spectra deconvolutions are the basis of the trends used for compositional predictions, Chromite-bearing lunar olivines require a modified approach to MGM deconvolutions. Such a modified approach has been developed by *Isaacson and Pieters* [2010], and involves truncating the olivine spectra to focus only on the 1000 nm region, as well as enforcing a flat (slope value of 0) continuum slope. This approach was able to reproduce the trends determined through analysis of terrestrial spectra lacking Cr-spinel absorptions [*Sunshine and Pieters*, 1998] to within ~5–10% accuracy. In addition to the Cr-spinel inclusions, lunar olivines studied with remote sensing may be affected by mixing with pyroxene. Pyroxene will introduce additional absorptions that complicate substantially deconvolutions of the composite olivine 1000 nm feature. Pyroxene and mixtures are discussed more thoroughly in section 5.2.3.

[7] The study by *Isaacson and Pieters* [2010] identified two major complications in compositional analyses of lunar

olivines with remotely sensed VNIR reflectance spectra: the long-wavelength absorptions caused by chromite inclusions and the effect of continuum slopes common to remotely sensed spectra of planetary surfaces. *Isaacson and Pieters* [2010] addressed the former complication but explicitly did not address the latter, limiting their analyses to laboratory reflectance spectra in which flat continuum slopes are appropriate. In this study, we extend the *Isaacson and Pieters* [2010] approach to address the effect of continuum slopes. We propose a method for standardizing the continuum slope used to deconvolve remotely sensed olivine spectra, and evaluate the effect of this method on the established trends in MGM-derived band position found in both terrestrial olivine and chromite-bearing lunar olivine spectra. We apply this approach to predict olivine compositions from several locations on the lunar surface using VNIR reflectance spectra collected by the Moon Mineralogy Mapper (M^3) on Chandrayaan-1 from several locations on the lunar surface.

2. Background: The Moon Mineralogy Mapper

[8] The Moon Mineralogy Mapper is an imaging spectrometer covering visible to near-infrared wavelengths. It was a guest instrument on the Indian Space Research Organisation (ISRO) Chandrayaan-1 mission. M^3 collected global data in 85 spectral channels from 400–3000 nm at a spatial resolution of 140 m/pixel from a 100 km orbit. More complete descriptions of the M^3 instrument are provided by *Pieters et al.* [2009, 2011]. A description of the calibration of M^3 data is provided by R. O. Green et al. (The Moon Mineralogy Mapper (M3) imaging spectrometer for lunar science: Instrument, calibration, and on-orbit measurement performance, submitted to *Journal of Geophysical Research*, 2011), and a description of the operational history and spatial coverage of M^3 is provided by *Boardman et al.* [2011].

3. Methods

3.1. Variable Continuum Slopes: Continuum Removal

[9] Continuum slopes in remotely sensed spectra are highly variable, as they can be influenced by a number of parameters, including surface texture, grain size, viewing geometry, and alteration such as through the process of space weathering. On the Moon, continuum slopes are predominantly affected by the presence of vapor-deposited nanophase iron-bearing rims on grains of lunar soil [e.g., *Pieters et al.*, 2000; *Hapke*, 2001; *Taylor et al.*, 2001; *Noble et al.*, 2005, 2007; *Taylor et al.*, 2010]. The optical effects of this nanophase iron are complex, but one of the major effects is an increase in the slope of the continuum (i.e., "red" continuum slopes). This effect becomes more pronounced with increasing degree of weathering [e.g., *Pieters et al.*, 2000; *Noble et al.*, 2001]. Even relatively immature materials on the Moon exhibit moderately "red" continuum slopes. Prominent continuum slopes cause shifts in apparent band center [e.g., *Clark and Roush*, 1984; *Clark*, 1999]. Thus, flat continuum slopes such as those used in previous systematic treatments of olivine reflectance spectra will not be practical for the majority of remotely sensed spectra collected of the lunar surface.

[10] The ubiquitous but variable nature of continuum slopes in remotely sensed VNIR reflectance spectra of planetary surfaces is a major complication in quantitative analysis of diagnostic absorption features present in those spectra. To treat these variable continuum slopes fully with an MGM-based approach, the continuum for each individual spectrum analyzed must be modeled individually for each fit [e.g., *Sunshine and Pieters*, 1998; *Sunshine et al.*, 2007]. While this is the most rigorous method to treat continuum slopes, the drawback of this approach is the additional complexity of the models and the potential variable methods applied to individual spectra. This variability can introduce more sources of error into comparisons between model results. To avoid these complexities and sources of error, we chose to use a systematic approach that will enable comparisons between model results more readily. We employ the approach developed by *Isaacson and Pieters* [2010] (truncating spectra and enforcing flat continuum slopes), but we include additional steps to address, in a systematic way, spectra for which flat continuum slopes are not practical.

[11] Our approach to dealing with continuum slopes is to remove the continuum slope prior to conducting MGM fits. This differs from the traditional MGM approach in which the continuum is modeled concurrently with the absorptions. Because the continuum is removed prior to performing deconvolutions, the slope (first-order polynomial term in the expression of the continuum slope) is fixed at zero for the deconvolutions, with only the offset (zero-order term) allowed to vary. We make a simplifying assumption that the relative trends in band position with olivine composition established from terrestrial olivines [*Sunshine and Pieters*, 1998] remain valid after continuum removal. However, it is beyond the scope of this project to verify that the effect of the continuum slope on band position is constant across all olivine compositions. Our goal in simplifying the modeling of the continuum slope is to ensure that we can apply our methods in a consistent manner regardless of the nature and magnitude of the continuum slope in any given spectrum. It is possible that our simplifications may introduce new biases, particularly if the effect of continuum removal is composition dependent. The advantage of this approach is that our methods can be replicated easily and consistently. However, a disadvantage of this approach is the inability to compare the resulting deconvolutions to existing deconvolutions of laboratory lunar olivine spectra performed without continuum removal. Thus, although the trends in band position with olivine composition are assumed to be valid in a relative sense, we cannot use our deconvolutions to assign absolute olivine compositions. A direct comparison to laboratory spectra would require substantial new laboratory work, including a reanalysis of the full suite of terrestrial laboratory olivine reflectance spectra with this new approach to modeling the continuum.

[12] The continuum slope to be removed is determined by fitting a local continuum over the principle olivine absorption feature. This local continuum slope is determined by tangent points on the short- and long-wavelength side of the absorption. Our method is to pick the "high reflectance" points on either side of the absorption as the tangent points. In our experience, the long-wavelength inflection point typically falls near ~1700 nm, while the short-wavelength

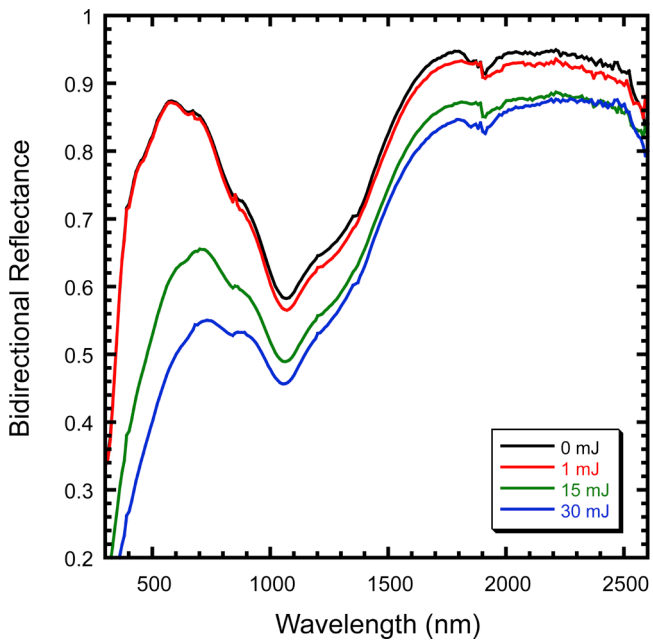

Figure 2. "Evaluation suite" laboratory reflectance spectra used to evaluate the effect of the continuum removal process on the MGM-derived band parameters. The samples are irradiated San Carlos (ISC) olivine subjected to varying degrees of laser energy as labeled in the lower right. Data are from *Yamada et al.* [1999].

inflection point is more variable. We evaluated continuum slope tangent points optimized for each spectrum as well as fixed tangent points for all spectra. We also evaluated various combinations of fixed and optimized tangent points (e.g., optimized short-wavelength point, fixed long-wavelength point for all spectra). While the differences are generally slight, we found that the results most consistent with established parameter ranges for olivine were obtained with short-wavelength tangent points optimized for each spectrum (though typically ~730–770 nm) and fixed long-wavelength tangent points at 1700 nm. Once obtained, the local continuum slope is "removed" by dividing the original spectrum by the local continuum. After performing the continuum removal based on these local continuum slopes, MGM fits are conducted as described by *Isaacson and Pieters* [2010]. As in the *Isaacson and Pieters* [2010] approach, in fitting a particular spectrum, multiple starting points are used to ensure that a "global" optimum fit is achieved. We employ the standard starting points presented by *Isaacson and Pieters* [2010], varying only the offset of the continuum slope in the starting models to a more reasonable value for continuum-removed spectra, which intersect zero in log reflectance space.

3.2. Effect of Continuum Removal: Laboratory Spectra

[13] We evaluate the robustness of the continuum removal process by analyzing its effect on deconvolutions of laboratory olivine reflectance spectra. The spectra used for these continuum removal analyses are a series of San Carlos olivine subsamples subjected to pulsed laser irradiation of varying intensity in an attempt to simulate the space weathering process [*Yamada et al.*, 1999; *Sasaki et al.*, 2002, 2003]. All of these subsamples have identical chemical compositions, and they vary only in the magnitude of laser irradiation to which they were exposed. This suite of laboratory spectra will be referred to as the "evaluation suite." This suite of spectra is plotted in Figure 2. The irradiated San Carlos (ISC) spectra are particularly useful for this evaluation because they exhibit a range of continuum slopes in spectra of an olivine of constant composition, and analysis by *Hiroi and Sasaki* [2001] using continuum slopes optimized for each individual spectrum suggests that the absorption bands do not move with increased irradiation (and increased continuum slope). Thus, these spectra allow us to evaluate the efficacy of our continuum removal approach, as any apparent band shift must be caused by the variable continuum slope, and our continuum removal approach must be able to correct for these apparent band shifts. Our procedure for evaluating the continuum removal process is to perform continuum removal on the evaluation suite using the method described above. An example of the continuum removal process is shown in Figure 3 for the spectrum of San Carlos olivine shown in Figure 1. A series of standard fits (based on the starting fits described by *Isaacson and Pieters* [2010], as discussed above) were then performed on the continuum-removed spectra as well as the original spectra, varying only the initial continuum offset to be appropriate for each case, as discussed above. As described above, the tangent points for definition of the local continuum slope were optimized individually for the short-wavelength point and fixed at 1700 nm for the long-wavelength point.

[14] After performing the described series of fits, the MGM-derived band centers of the continuum-removed and original spectra (from the same fits) were then compared, and were used to calculate a predicted composition (Fo #) using the approach of *Isaacson and Pieters* [2010]. This comparison is performed to gauge the effectiveness of our continuum removal procedure at "standardizing" the continuum slope modeling, and to evaluate the compositional modeling in the context of the standard trends presented previously [*Sunshine and Pieters*, 1998; *Isaacson and Pieters*, 2010]. The absolute calibration of this procedure will not "match" that of the standard terrestrial analyses [*Sunshine and Pieters*, 1998] due to the different continuum approach used. However, the relative trends in band position with composition are still valid (the absorptions move absolutely as a function of the olivine chemistry, and the linear continuum slope removal should only produce an apparent offset in band positions). This means that our approach cannot be used to evaluate absolute olivine composition based on previous laboratory analyses [*Sunshine and Pieters*, 1998; *Isaacson and Pieters*, 2010] but can be used to make relative compositional predictions (Mg-rich versus Fe-rich relative to other spectra analyzed in the same manner).

3.3. Application to M^3 Spectra

[15] These procedures (continuum removal, MGM fits, relative compositional prediction) were applied to a suite of olivine-dominated reflectance spectra collected by the M^3 in its low-resolution mode of 140 m/pixel spatial resolution and 20–40 nm spectral resolution. Here, we focus on a suite of olivine-dominated spectra collected from select regions

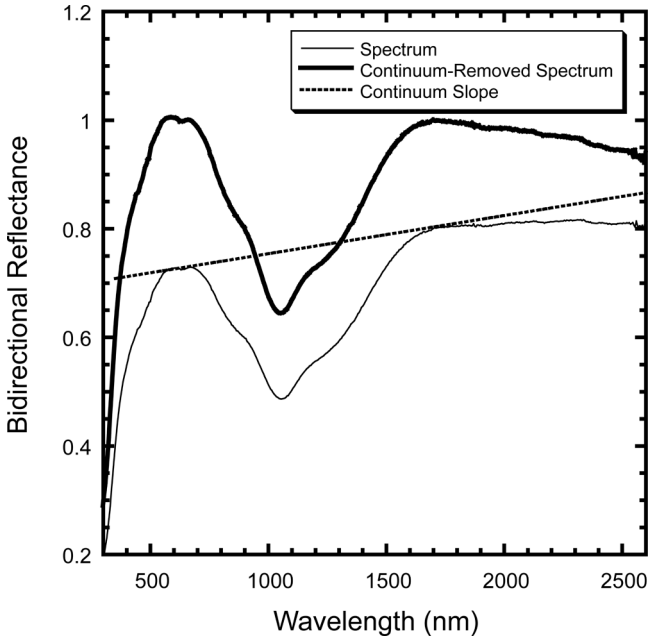

Figure 3. Demonstration of the continuum removal process using a local continuum slope tangent on either side of the principal absorption feature, with the long-wavelength point fixed at 1700 nm and the short-wavelength point variable depending on the spectrum. The short-wavelength tangent point for this spectrum is at 665 nm. The thin line is the original spectrum, the dashed line is the local continuum slope, and the heavy line is the continuum-removed spectrum. The long-wavelength slope in the continuum-removed spectrum is negative because the continuum slope is steeper than the original spectrum in this wavelength region.

on the lunar surface. These regions include a small crater northwest of the rim of the Moscoviense basin, the Copernicus central peak, Aristarchus, and Marius crater in the eastern Marius Hills. Previous studies have identified the presence of olivine at Copernicus [*Pieters*, 1982; *Pieters and Wilhelms*, 1985; *Lucey et al.*, 1991; *Le Mouélic*, 2001; *Yamamoto et al.*, 2010] and Aristarchus [*Le Mouélic et al.*, 1999a; *Chevrel et al.*, 2009; *Yamamoto et al.*, 2010]. The Moscoviense olivines occur close to exposures of unusual mafic lithologies [*Pieters et al.*, 2011] and may be associated with the processes responsible for the production of those lithologies, although our analyses cannot confirm a genetic relationship. Olivine-rich areas were highlighted by using a ratio of the integrated band strengths at 1000 and 2000 nm. In our formulation (1000 nm/2000 nm), spectra with strong 1000 nm features and weak 2000 nm features, such as those dominated by olivine, will have high values in this parameter. This approach is highlighted in Figure 4, which shows this parameter mapped in color overlaid on a M^3 albedo band for context. Two regions are displayed in Figure 4, the small crater in the Moscoviense region and Copernicus. Areas showing up in yellow-orange-red colors in this scheme will tend to be olivine-rich. The olivine spectra from Aristarchus are discussed by *Mustard et al.* [2011], and those from Marius are discussed by *Besse et al.* [2011]. The Aristarchus olivines are located in the southwest rim and ejecta of Aristarchus, and the Marius olivines are located in the floor of the crater Marius, which is located on the eastern boundary of the Marius Hills complex. A number of spectra were extracted, although only the "best" (most pure olivine signature) were selected for MGM fitting. Unless otherwise noted, spectra were extracted as averages of 3 × 3 spatial pixels. Fits were performed on continuum-removed spectra. While most analyses presented here used continuum tangent points of ~730 nm and ~1700 nm, these should not be used universally for remotely sensed olivine spectra; we have observed numerous spectra for which these tangent points

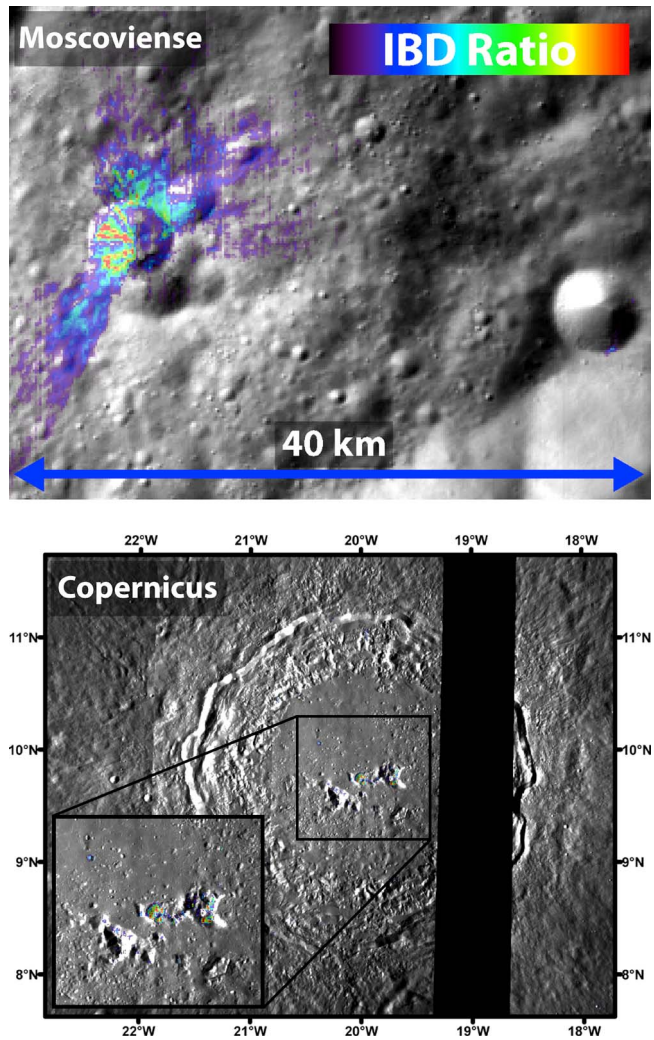

Figure 4. Integrated band depth ratio images for (top) small crater northwest of Mare Moscoviense and (bottom) Copernicus. Color overlay is a ratio of the integrated band depths (IBD) over the 1000 and 2000 nm ferrous absorption features. High values indicate spectra with strong 1000 nm and weak 2000 nm absorptions, suggestive of olivine-rich lithologies. In order to show only the strongest detections, areas falling below a threshold value were not colored. These maps were used as a guide to select some of the olivine-dominated reflectance spectra analyzed in this study. The base image is a single M^3 band near 3000 nm that is sensitive to morphology. The Moscoviense image (Figure 4, top) is ~40 km across, and the diameter of Copernicus is ~93 km [*Andersson and Whitaker*, 1982].

Table 1. Local Continuum Slope Parameters for Evaluation Suite Spectra

Sample[a]	Tan λ Short[b]	Tan λ Long[b]	Slope[c]	Intercept
ISC 0	580	1700	5.42	0.843
ISC 1	580	1700	4.24	0.848
ISC 15	700	1700	20.0	0.516
ISC 30	730	1700	28.7	0.341

[a]ISC, Irradiated San Carlos (numbers refer to pulse laser intensity, higher indicating greater degree of irradiation).
[b]Tan stands for tangent.
[c]Continuum slope removed from spectrum. Slope × 10^5. Units are reflectance/λ, λ in nm.

would be inappropriate. As was done with the laboratory spectra, a range of starting points for the deconvolutions were employed, to test the sensitivity of the results to starting model conditions. In our evaluation of the results of fits to these spectra, we disregard effects of temperature, as the range in surface temperature for the observations is reasonably small (~40 K). However, it is well documented, both from theory [e.g., *Burns*, 1970, 1993] and observation [e.g., *Aronson et al.*, 1970; *Singer and Roush*, 1985], that increased temperatures can lead to broadened absorption features, particularly for the long-wavelength (M1-2) olivine absorption. Thus, potential temperature effects should be considered an additional, though comparatively minor, source of error.

3.3.1. Data Corrections

[16] Because noise in reflectance spectra can degrade the quality of MGM fits, we performed mild spectral corrections prior to MGM deconvolutions. These corrections are intended to suppress minor, residual band-to-band calibration artifacts in M^3 spectra. We chose to use a correction based on the assumption that lunar reflectance spectra should be smoothly varying band-to-band at the M^3 spectral sampling (i.e., that sharp, spike-like features are artifacts rather than real features, particularly in the 1000 nm region where the olivine absorptions are found). The correction factors are derived by evaluating a suite of "featureless" spectra that exhibit very weak absorption features (largely mature highland soils) and forcing them to be as smooth as possible at the M^3 spectral sampling. These correction factors were applied to all spectra evaluated in this study. To ensure that no bias was introduced by this correction, we performed identical fits on "original" and "corrected" M^3 spectra and evaluated the results. Two M^3 spectra from the suite evaluated in this study were selected for this analysis, and the relative predicted compositional variation compared between the "original" and "corrected" spectra. The relative predicted compositional variation between the spectra differed by less than one Fo # unit between the "original" and "corrected" spectra, indicating that relative compositional predictions are not affected by this correction step.

3.3.2. Error Analysis

[17] The approach used to evaluate olivine composition with M^3 spectra presents a number of sources of error. While we have already addressed the inability of our approach to predict compositions absolutely, there are additional sources of error in the shift between high-quality laboratory spectra and spectra acquired from lunar orbit. The M^3 spectra have a lower signal-to-noise ratio and spectral resolution than laboratory data. The MGM is also subject to errors resulting from variable model initial conditions. *Isaacson and Pieters* [2010] found that variable starting MGM conditions led to an error of ~5 Fo # (Mg/(Mg+Fe)) units for laboratory olivine spectra. In their analyses of pyroxenes, *Kanner et al.* [2007] found that such uncertainties are substantially magnified in remotely sensed data relative to laboratory data. To evaluate the effect of these error sources, we performed a series of MGM fits to a single M^3 spectrum extracted from the Moscoviense area with a wide array of model initial conditions. Plots and more details are provided in section 4.2. We analyzed the results of each olivine absorption individually, taking the maximum and minimum band position and calculating a range in band position (this gives the "error" in the band center dimension). The maximum and minimum band center wavelengths were used to calculate a range in predicted Fo # using the trend line for the specific absorption, producing the error in the relative predicted Fo # dimension. The trends in band center wavelength versus composition are discussed by *Sunshine and Pieters* [1998] and *Isaacson and Pieters* [2010]. To calculate a composite error for the three bands treated together, the Fo # was calculated for all three bands simultaneously for all of the error analysis fits performed to the M^3 spectrum. The maximum and minimum predicted Fo # were used to estimate a range in predicted composition, producing the composite error in the Fo # dimension. There is no composite error in the band center dimension, as all three bands were evaluated simultaneously to evaluate the composite error in Fo #.

4. Results

4.1. Laboratory Spectra

[18] The selected tangent points and the parameters for the local continuum removed from the laboratory evaluation suite spectra are provided in Table 1. The continuum removal process for these spectra is illustrated in Figure 5. Example fits to the evaluation suite are illustrated in Figure 6. Full results of the MGM analyses of the evaluation suite, both original and continuum removed based on the parameters in Table 1, are reported in Tables 2 (original) and 3 (continuum removed). The multiple entries for each spectrum refer to the various starting points for the MGM. High and low initial continuum offsets were evaluated to test the effect of diverse starting continuum offsets. As discussed above, a range of initial parameters were evaluated, although only those parameters that were the most logical and consistent with the evaluation suite spectra are reported here. Band centers for both sets are compared directly in Table 4, with continuum removal parameters from Table 1 provided for reference.

[19] The MGM-derived band centers for fits to the ISC spectra, as illustrated by the examples in Figure 6, are plotted against the relative composition as predicted from the methods of *Isaacson and Pieters* [2010] in Figure 7. Fits to the original (not continuum removed) spectra span a range in band center wavelengths, with the more steeply sloped spectra (15 and 30 mJ) exhibiting band centers at shorter wavelengths. This is consistent with theory and previous results, as a red-sloped continuum (increasing reflectance with wavelength) causes bands to be apparently shifted to shorter wavelengths [e.g., *Clark and Roush*, 1984;

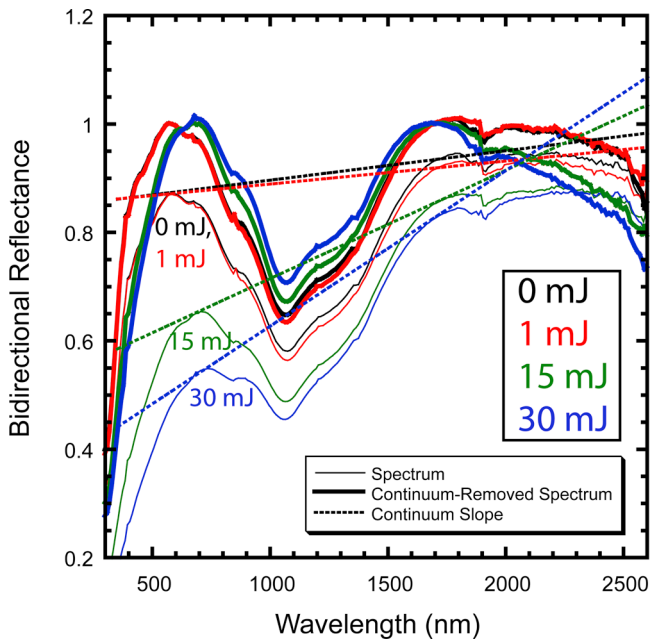

Figure 5. Continuum removal process for the evaluation suite spectra presented in Figure 2. The line style scheme is the same as in Figure 3, and the color/line scheme is as labeled (same as Figure 2). Note the range of continuum slopes exhibited by these spectra. The tangent points used to derive the local continuum slope are indicated in Table 1.

Clark, 1999]. Fits to the continuum-removed spectra, however, exhibit band centers clustered at essentially the same wavelength. Recall that the composition of the olivine is identical (~Fo_{90}) for each spectrum evaluated in this analysis.

4.2. M^3 Spectra

[20] Examples of M^3 spectra collected from olivine-rich areas, as highlighted by Figure 4, are plotted in Figure 8. Examples of the extracted M^3 spectra are compared to several of the evaluation suite spectra as well as terrestrial (Fo_{90}) and synthetic (Fo_{60}) laboratory spectra in Figure 9. The spectra in Figure 9 have been normalized by the maximum band strength such that the absorption feature of each spectrum ranges from zero to one. This approach was used previously by *Lucey* [1998] and *Sunshine et al.* [2007]. The spectra are shown on identical axes (Figure 9a) as well as offset for enhanced clarity (Figure 9b). The continuum removal used is slightly different from that applied in our modeling approach. The continuum removal used in Figure 9 is that typically applied to telescopic spectra, with tangent points at 730 nm and 1600 nm [e.g., *Pieters*, 1986], which enables more easy comparison to other published studies but does not alter substantially the observed spectral properties, as it is similar to continuum slopes used for continuum removal in this study.

[21] Example MGM fits to the spectra shown in Figure 8 are illustrated in Figure 10. It should be noted that more spectra were evaluated than are shown in Figures 8–10 (only one spectrum is displayed from each region we evaluated in each case), but the spectra shown in Figures 8–10 are representative of the suite. The slopes removed from the M^3 spectra prior to performing the MGM fits are reported in Table 5. The discontinuous numbering for some of these spectra is due to the subsetting of a larger set of M^3 spectra prior to performing MGM fits (fits were performed only for the "best" spectra). The full results of the MGM fits to the M^3 spectra for the spectra lacking evidence for other nonolivine absorbing phases (Moscoviense and Copernicus) are reported in the auxiliary material.[1] As was done with the laboratory spectra, a range of starting points for the deconvolutions were employed. We report only the results from the intermediate starting point, as it allows more freedom for the fit to converge on the best result. The results of predicting the relative olivine composition are shown in Figure 11, a plot of MGM-derived band position versus relative predicted composition, similar to the scheme used for Figure 7. The large tick marks on the *y* axis of Figure 11 represent 20 relative Fo # units. Also plotted on Figure 11 are the band centers and relative predicted composition for fits to the continuum-removed evaluation suite spectra for comparison, as well as the error range brackets for individual absorptions (labeled) and the composite relative Fo # prediction error range bracket derived as described in section 3. The M^3 spectrum used to derive these range brackets is the Moscoviense spectrum illustrated in Figure 8. The range in relative predicted composition ("Composite Error") is approximately 20 in Fo # (Mg′ = molar Mg/(Mg+Fe)). Data points are not shown for the Aristarchus and Marius olivines, as we believe these spectra are affected by phases in addition to olivine (that they are not totally olivine dominated), as discussed below. Full results of MGM deconvolutions of the Moscoviense and Copernicus M^3 spectra are reported in the auxiliary material.

5. Discussion

5.1. Effect of Continuum Removal: Laboratory Spectra

[22] Examples of fits to the original and continuum-removed laboratory spectra are shown in Figure 6, and full results of the MGM fits are reported in Tables 2 and 3. While a wide range of initial MGM parameters were used to capture the systematics fully, we report only those starting points most consistent with the compositions of the laboratory spectra analyzed, as they are the most robust and consistent with the a priori knowledge of these samples and spectra. Before discussing band center results, note the effect of continuum removal on relative band strengths in Figure 6. This is particularly apparent in the 15 mJ spectrum, which exhibits a fairly pronounced local continuum slope. Prior to continuum removal, the M1-1 band is disproportionately strong based on relative band strengths determined for terrestrial olivine spectra [*Sunshine and Pieters*, 1998]. This disproportionate band strength is due to the use of a flat continuum slope in the deconvolution, which necessitates a stronger M1-1 absorption to account for the sloped nature of the spectrum. Continuum removal brings the relative band strengths more into agreement with the anticipated trends from laboratory analyses. While difficult to see in plots such as Figure 6, systematic differences in the MGM-derived band positions are observed between

[1]Auxiliary materials are available in the HTML. doi:10.1029/2010JE003731.

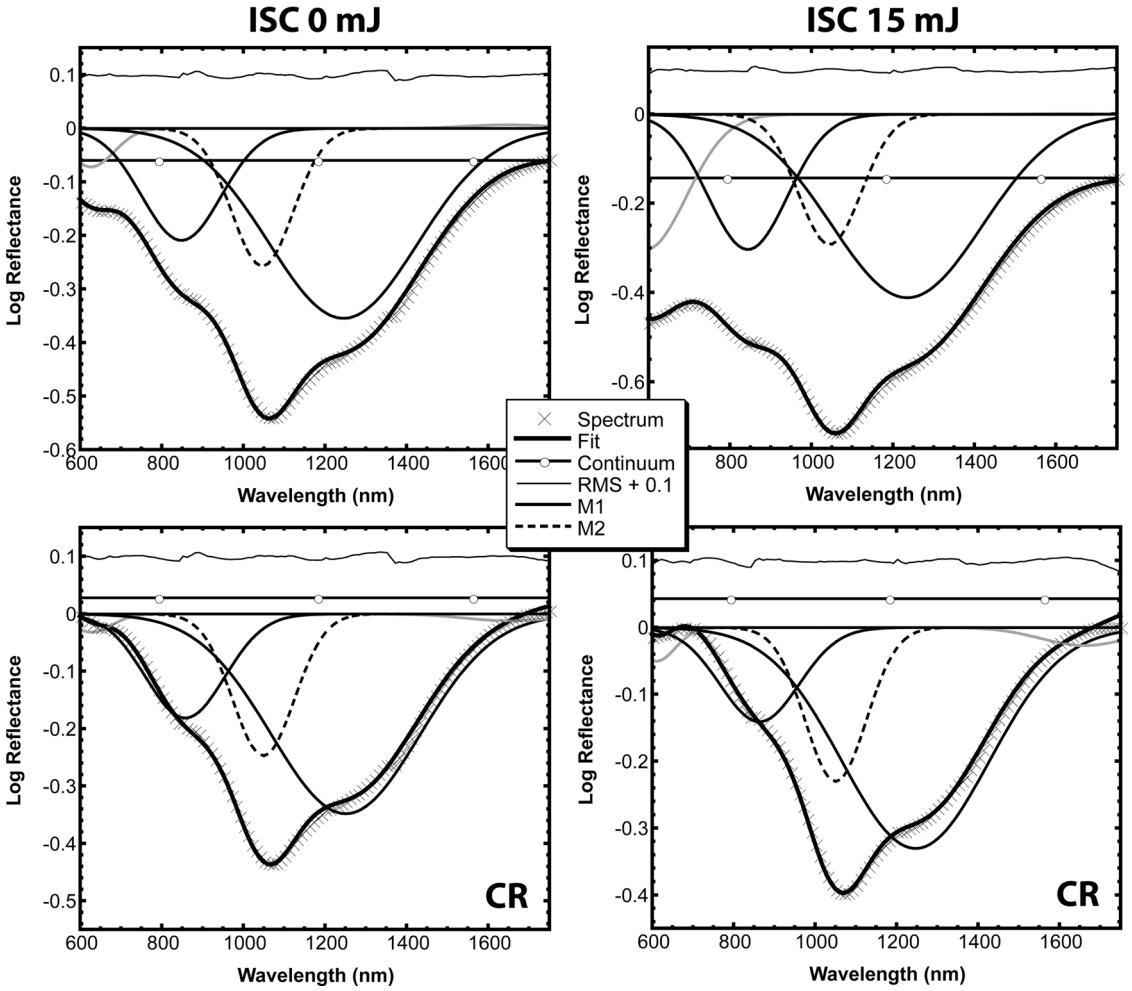

Figure 6. Example MGM fits to selected spectra from the evaluation suite (Figures 3 and 5). (top) Original spectra and (bottom) continuum removed, labeled with "CR." (left) Fits to spectra of the original (not irradiated) sample and (right) fits to the ISC 15 mJ spectra. Note the differing continuum slopes between 0 and 15 mJ prior to continuum removal, leading to a disparity in relative band strengths that is resolved after continuum removal. These fits were all produced from the same MGM starting point, with only the continuum offset adjusted.

fits to continuum-removed and fits to noncontinuum-removed spectra. The results presented in Tables 2 and 3 are condensed in Table 4, which reports only band centers for the three principal absorptions and the slope of the local continuum removed.

[23] The MGM-derived band centers for fits to the evaluation suite spectra are presented in Figure 7, a plot of these band positions versus relative composition as predicted from the band centers. Figure 7 illustrates the importance of treating the continuum slope appropriately. The use of the flat continuum slope on the original (not continuum removed) spectra clearly introduces an apparent shift in band centers to shorter wavelengths with increasing spectral slope, as evidenced by the spread in the band center wavelengths and predicted compositions for the "original" spectra. Continuum removal using our approach, however, causes the MGM-derived band centers to cluster around nearly identical wavelengths. This is an important proof of concept for the continuum removal approach: the evaluation suite spectra differ only in the degree to which the samples have been exposed to the laser irradiation. The compositions of the samples are identical. Thus, the fact that the continuum-removed results are nearly identical for the full suite suggests that our continuum removal process is successful at negating the effects of variable continuum slopes and will allow compositional predictions in a relative sense. The similarity of the spectra after continuum removal is further illustrated by Figure 9, which demonstrates that after correcting for spectral contrast differences, the evaluation suite exhibits highly similar spectral properties between the original (0 mJ) and most severely irradiated (30 mJ) samples. The derived band centers for the evaluation suite spectra are compared to the band centers derived for the M^3 spectra in Figure 11. It is tempting to use the absolute composition of the evaluation suite to "benchmark" the relative results for the M^3 spectra. However, the derivation of absolute compositions would then be based effectively on a single data point, so substantial caution should be employed. Nevertheless, if all of the precautions discussed in this paper are weighed carefully (including the limitations

Table 2. MGM Results for Fits to the Evaluation Suite Spectra Without Continuum Removal

	M1-1			M2			M1-2		
Starting Point[a]	Center[b]	FWHM[c]	Intensity[d]	Center[b]	FWHM[c]	Intensity[d]	Center[b]	FWHM[c]	Intensity[d]
				ISC 0 mJ Spectrum					
Mg High	847.6	228.4	−0.209	1046.0	177.7	−0.257	1244.7	428.0	−0.354
Int. High	847.9	228.6	−0.210	1046.1	177.8	−0.258	1245.2	427.4	−0.355
Mg Low	847.9	228.2	−0.204	1046.0	176.9	−0.254	1243.5	426.7	−0.349
Int. Low	848.1	228.3	−0.205	1046.1	177.0	−0.255	1244.1	426.1	−0.350
				ISC 1 mJ Spectrum					
Mg High	850.5	228.5	−0.208	1046.1	177.9	−0.260	1242.2	428.7	−0.371
Int. High	850.8	228.6	−0.209	1046.2	178.0	−0.261	1242.6	428.1	−0.372
Mg Low	850.8	228.3	−0.204	1046.1	177.2	−0.258	1241.4	427.4	−0.367
Int. Low	851.0	228.4	−0.205	1046.2	177.3	−0.259	1241.9	426.8	−0.367
				ISC 15 mJ Spectrum					
Mg High	843.1	230.0	−0.303	1043.9	181.5	−0.291	1234.5	435.0	−0.411
Int. High	843.4	230.1	−0.303	1044.0	181.6	−0.292	1234.8	434.3	−0.411
Mg Low	841.3	229.8	−0.290	1043.4	181.0	−0.282	1230.8	434.6	−0.397
Int. Low	841.6	229.9	−0.291	1043.6	181.1	−0.283	1231.3	433.9	−0.397
				ISC 30 mJ Spectrum					
Mg High	843.1	231.1	−0.356	1042.8	184.1	−0.309	1229.1	438.4	−0.420
Int. High	843.3	231.3	−0.355	1042.9	184.2	−0.309	1229.3	437.7	−0.419
Mg Low	840.9	230.9	−0.344	1042.2	183.3	−0.298	1224.3	437.3	−0.404
Int. Low	841.1	231.0	−0.344	1042.3	183.4	−0.299	1224.6	436.6	−0.403

[a]Starting point for MGM fit. Mg/Int. refers to band positions (Mg-rich, intermediate) following the *Isaacson and Pieters* [2010] approach. High/low refers to initial continuum offset.
[b]Band centers reported in nm.
[c]FWHM values in nm.
[d]Intensity reported as natural log reflectance.

of the approach in comparisons to terrestrial data discussed in section 3.1 and the reduced accuracy relative to analyses of laboratory data), and the data are fully calibrated (Green et al., submitted manuscript 2011), corrected for photometry [e.g., *Hicks et al.*, 2011], and corrected for thermal emission [e.g., *Clark et al.*, 2011] (all of which are part of ongoing efforts by the M^3 team), then deconvolutions of M^3 olivine-dominated spectra can be used to obtain absolute olivine compositions. Evaluation of a range of terrestrial olivine compositions subjected to laser irradiation in a similar

Table 3. MGM Results for Fits to the Evaluation Suite Spectra After Continuum Removal

	M11			M2			M1-2		
Starting Point[a]	Center[b]	FWHM[c]	Intensity[d]	Center[b]	FWHM[c]	Intensity[d]	Center[b]	FWHM[c]	Intensity[d]
				ISC 0 mJ Spectrum					
Mg High	856.6	228.2	−0.181	1048.5	177.7	−0.247	1250.2	427.7	−0.348
Int. High	856.7	228.3	−0.182	1048.6	177.8	−0.248	1250.6	427.1	−0.348
Mg Low	857.6	227.9	−0.179	1048.6	176.5	−0.245	1249.7	426.2	−0.345
Int. Low	857.7	228.0	−0.180	1048.8	176.7	−0.246	1250.1	425.5	−0.345
				ISC 1 mJ Spectrum					
Mg High	857.8	228.3	−0.185	1048.0	177.7	−0.251	1246.0	428.2	−0.364
Int. High	858.0	228.4	−0.186	1048.1	177.9	−0.252	1246.5	427.7	−0.364
Mg Low	858.8	227.9	−0.184	1048.2	176.6	−0.250	1245.8	426.4	−0.362
Int. Low	859.0	228.1	−0.184	1048.3	176.7	−0.251	1246.2	425.9	−0.362
				ISC 15 mJ Spectrum					
Mg High	862.7	227.8	−0.141	1049.8	176.3	−0.230	1246.0	425.1	−0.330
Int. High	862.6	227.9	−0.142	1049.8	176.4	−0.231	1246.6	424.5	−0.331
Mg Low	864.6	227.7	−0.136	1050.0	175.9	−0.226	1244.6	424.8	−0.325
Int. Low	864.7	227.7	−0.137	1050.1	175.9	−0.227	1245.1	424.0	−0.326
				ISC 30 mJ Spectrum					
Mg High	858.2	227.7	−0.110	1049.7	175.8	−0.213	1245.2	423.0	−0.287
Int. High	858.0	227.7	−0.112	1049.8	175.9	−0.215	1246.1	422.4	−0.288
Mg Low	860.7	227.6	−0.101	1049.8	175.7	−0.205	1241.4	423.8	−0.280
Int. Low	861.1	227.7	−0.102	1049.9	175.6	−0.206	1242.0	422.9	−0.280

[a]Starting point for MGM fit. Mg/Int. refers to band positions (Mg-rich, intermediate) following the *Isaacson and Pieters* [2010] approach. High/low refers to initial continuum offset.
[b]Band centers reported in nm.
[c]FWHM values in nm.
[d]Intensity reported as natural log reflectance.

Table 4. Comparison of MGM-Derived Band Centers for Evaluation Suite Spectra, With and Without Continuum Removal

Fit	Center M1-1	Center M2	Center M1-2	Center CR[a] M1-1	Center CR[a] M2	Center CR[a] M1-2	Continuum Slope[b]	Continuum Intercept
				ISC 0 mJ Spectrum				
Mg High	847.6	1046.0	1244.7	856.6	1048.5	1250.2	5.42	0.843
Int. High	847.9	1046.1	1245.2	856.7	1048.6	1250.6		
Mg Low	847.9	1046.0	1243.5	857.6	1048.6	1249.7		
Int. Low	848.1	1046.0	1244.1	857.7	1048.8	1250.1		
				ISC 1 mJ Spectrum				
Mg High	850.5	1046.1	1242.2	857.8	1048.0	1246.0	4.24	0.848
Int. High	850.8	1046.2	1242.6	858.0	1048.1	1246.5		
Mg Low	850.8	1046.1	1241.4	858.81	1048.2	1245.8		
Int. Low	851.0	1046.2	1241.9	859.0	1048.3	1246.2		
				ISC 15 mJ Spectrum				
Mg High	843.1	1043.9	1234.5	862.7	1049.8	1246.0	20.0	0.516
Int. High	843.4	1044.0	1234.8	862.6	1049.8	1246.6		
Mg Low	841.3	1043.4	1230.8	864.6	1050.0	1244.6		
Int. Low	841.6	1043.6	1231.3	864.7	1050.1	1245.1		
				ISC 30 mJ Spectrum				
Mg High	843.1	1042.8	1229.1	858.2	1049.7	1245.2	28.7	0.341
Int. High	843.3	1042.9	1229.3	858.0	1049.8	1246.1		
Mg Low	840.9	1042.2	1224.3	860.7	1049.8	1241.4		
Int. Low	841.1	1042.3	1224.6	861.1	1049.9	1242.0		

[a]CR, continuum removed.
[b]Continuum slope removed from spectrum. Slope × 10^{-5}. Units are reflectance/λ, λ in nm.

manner to the evaluation suite would be a logical area of additional research. Such work would enable the methods presented here to predict absolute olivine compositions much more reliably.

5.2. Application to M^3 Spectra

[24] We performed continuum removal on the M^3 spectra with the same method used for the laboratory spectra. The results of MGM deconvolutions to these spectra are reported in the auxiliary material, with only the results of the intermediate starting point reported, as discussed in section 4. Example fits, to the same example M^3 spectra shown in Figure 8, are shown in Figure 10. Immediately apparent is the higher level of "noise" in the M^3 spectra relative to laboratory spectra, as evidenced by the high-frequency variation in the input spectra (gray X's). Also apparent is the

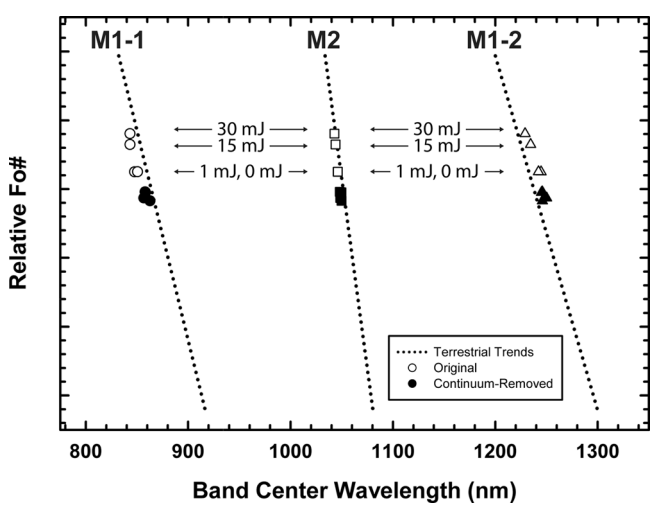

Figure 7. MGM-derived band centers and relative predicted compositions for the evaluation suite spectra. The evaluation suite spectra without continuum removal ("original") span a range of band center wavelengths and predicted compositions, but all samples have the same absolute olivine composition (Fo #). The continuum-removed results cluster around the same band center wavelength and relative predicted composition, demonstrating the viability of our continuum removal process.

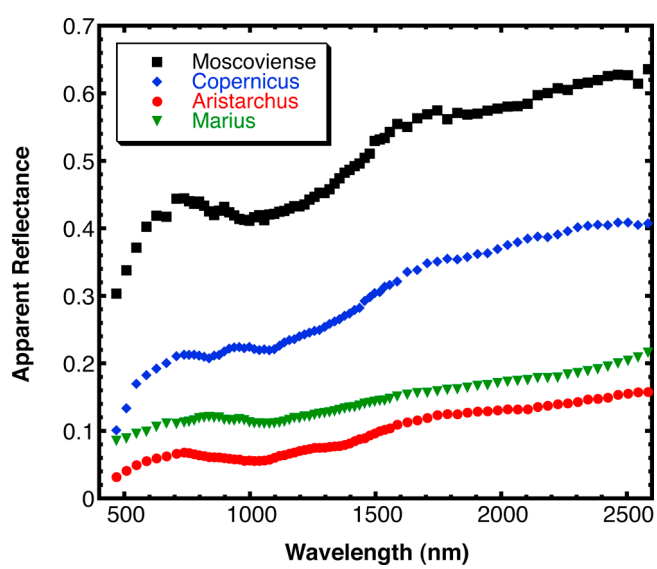

Figure 8. Example M^3 spectra collected from each region analyzed. These do not make up the full suite of spectra analyzed but are indicative of typical olivine-rich spectra collected from each region. The spectra have been truncated at 2600 nm to enable direct comparison with laboratory spectra.

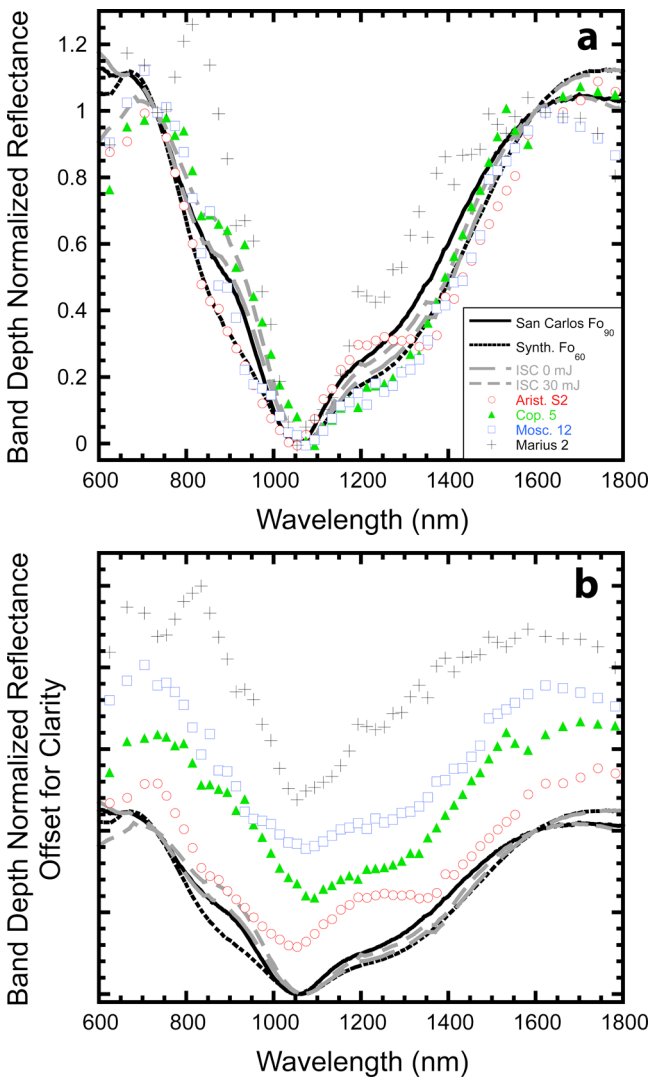

Figure 9. Comparison of olivine spectra. Representative example M^3 spectra from each suite evaluated are plotted, as are example laboratory spectra (Fo_{90} and Fo_{60}) and two of the evaluation suite spectra (0 mJ and 30 mJ). The Fo_{60} spectrum is discussed by *Dyar et al.* [2009]. The spectra are shown after continuum removal and normalization such that the band strength ranges from zero to one for all spectra, eliminating complications such as variable albedo, spectral contrast, and slope. Spectra are shown (a) on the same axes and (b) offset for clarity.

reduced spectral sampling of M^3 across this wavelength region (20 nm). These factors combine to produce noisier fits, as indicated by the RMS error line. Relative to fits to the continuum-removed laboratory spectra, higher continuum offsets were used for fits to the M^3 spectra. We experimented with a range of offset values, and found that for these spectra, a higher offset value allowed the individual Gaussians more freedom to move and converge on the appropriate fit result. Note also the apparent errors in the fit at extreme short and especially extreme long wavelengths. This is a byproduct of the high continuum offset and the use of only one Gaussian to model the outer (extreme short and long) wavelengths. This is inconsequential to the MGM results for the three principal olivine absorptions. The angularity of the Gaussians (and consequentially of the spectral fit) is a product of the reduced spectral sampling of the M^3 spectra in comparison to the laboratory spectra (5 nm).

[25] The reduced spectral sampling and increased noise levels in M^3 spectra relative to laboratory spectra mean that the compositional predictions based on MGM deconvolutions of the M^3 spectra must be interpreted with caution. Even though we only evaluate composition in a relative sense, the relatively low spectral sampling make the MGM analyses fairly sensitive to noise, especially for olivine absorptions. Olivine absorptions shift a maximum of ~70 nm over the full compositional range (Fo_{100} to Fo_0), equivalent to ~3.5 M^3 spectral channels in the maximum spectral resolution used in this study (Green et al., submitted manuscript, 2011). Substantial errors in even a few channels due to noise, especially if noise causes spurious features spanning several channels, can introduce serious biases in the fit results. Even in analyzing telescopic data of asteroids with higher signal levels and spectral sampling, *Sunshine et al.* [2007] classified olivine compositions into only three broad groups. Despite these cautions, the M^3 data analyzed here do show clear spectral variability, as discussed below, and this variability was quantified with the MGM.

5.2.1. Qualitative Spectral Diversity

[26] Representative examples of the spectra analyzed in this study are illustrated with common continuum removal and scaled absorption magnitudes in Figure 9. This scaling approach allows true spectral variability to be evaluated more easily, as it eliminates complicating factors such as variable spectral contrast, albedo, and continuum slope. While Figure 9a is the most useful for absolute comparisons, Figure 9b shows the individual spectra more clearly, reducing clutter. Figure 9 illustrates that there are spectral differences between the suites of olivines analyzed. The Moscoviense and Copernicus olivines are fairly similar, although the Moscoviense olivine spectrum plotted in Figure 9 exhibits a slightly broader long-wavelength absorption that the Copernicus spectrum. However, the Copernicus spectrum in this region may be biased by the sharp feature near 1500 nm that gives the illusion of a strong but relatively narrow long-wavelength absorption. This sharp feature near 1500 nm is in the spectral region of a filter boundary on the M^3 detector (Green et al., submitted manuscript, 2011) and thus likely is not a "real" feature. The Copernicus spectra also exhibit a fairly sharp "dip" in reflectance near ~850 nm that is observed consistently across the Copernicus suite and likely is not "real." This feature will influence the MGM deconvolutions. The Moscoviense olivines were observed to be more spectrally diverse than the Copernicus olivines, which are remarkably homogeneous. The Aristarchus and Marius spectra exhibit prominent differences from the Copernicus and Moscoviense olivine spectra.

[27] The Aristarchus spectrum exhibits a prominent feature near 1300 nm. A feature of this relative magnitude at this wavelength is inconsistent with pure olivine [*Burns*, 1970; *Sunshine and Pieters*, 1998], although very Fe-rich olivines do tend to exhibit stronger long-wavelength (M1-2) absorptions [*Sunshine and Pieters*, 1998]. However, the Aristarchus spectrum exhibits a relatively short-wavelength band minimum, which would be at odds with a very Fe-rich

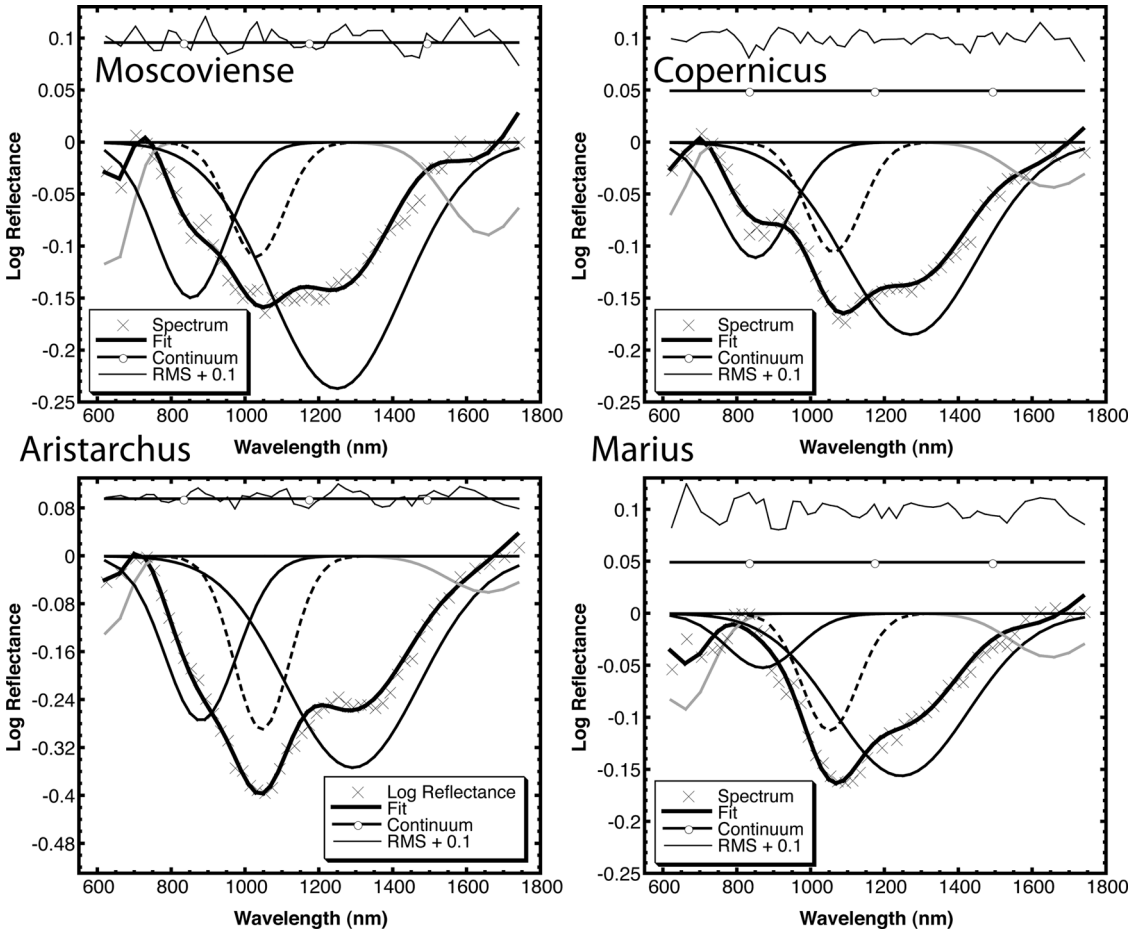

Figure 10. Example MGM fits to continuum-removed M^3 spectra. The examples shown are fits to the same spectra shown in Figure 8 after applying our continuum removal approach. The same labeling scheme is used as in Figure 6. The angular nature of the Gaussians is a product of the reduced spectral sampling of M^3 relative to laboratory data. The higher offset values as compared to fits to the evaluation suite spectra are discussed in the text. The increased "noise" in the fits is a product of the reduced spectral sampling and increased noise of the M^3 data relative to laboratory spectra. The poor fits of these spectra at long wavelengths are a product of higher continuum offsets and modeling the long-wavelength region with only one Gaussian and are inconsequential to the results for the critical component absorptions of the 1000 nm feature.

composition, and the 1300 nm absorption appears inconsistent with pure olivine. Furthermore, very Fe-rich olivines (below ~Fo_{50}) are not found in the lunar sample collection in sufficient abundances to be detectable with remote VNIR reflectance spectroscopy. While difficult to interpret compositionally, the Aristarchus spectra do suggest a different geologic context for the olivine. It is possible that the Aristarchus olivines were formed as a crystallization product of a melted basalt source, as the olivines at Aristarchus appear to be associated largely with impact melt-derived materials [*Mustard et al.*, 2011]. The melted basalt source may help explain the presence of pyroxene or other phases that artificially strengthen the M1-2 absorption relative to the other olivine absorptions. Fe-bearing glass is a potential such contaminant, and would not be unexpected in the Aristarchus region, particularly in association with impact melt-derived materials [*Le Mouélic et al.*, 1999b; *Mustard et al.*, 2011]. Very Fe-rich plagioclase (greater than ~0.25 wt % FeO) is another possibility [e.g., *Adams and Goullaud*, 1978; *Isaacson et al.*, 2011]. However, it would be surprising for either of these candidate phases to exhibit such a pronounced spectral feature in the presence of abundant olivine, which otherwise dominates the spectrum. Regardless of the origin of the spectral differences between Aristarchus and the other spectra analyzed, the observed differences suggest that the Aristarchus olivines were formed by a different geologic process than that responsible for the olivines at Moscoviense and Copernicus.

[28] The Marius spectrum also differs from the Copernicus and Moscoviense spectra. It is substantially narrower in the 1000 nm region, exhibiting weaker short-and long-wavelength (olivine M1) absorptions. It also exhibits a fairly short-wavelength band minimum, closer to that of the Aristarchus spectrum. While not apparent from Figure 9, which highlights the 1000 nm region, the Marius olivine spectra do exhibit 2000 nm absorptions, which could be caused by chromite inclusions or mixtures with pyroxene. The association of the Marius olivines with basalts and the

Table 5. Local Continuum Slopes Removed From M^3 Spectra Prior to MGM Fits

Spectrum	Continuum Slope[a]	Continuum Offset	Tan λ Short[b]	Tan λ Long[b]
Mosc-9	9.80E-05	0.317	730	1700
Mosc-12	8.80E-05	0.248	730	1700
Mosc-16	1.57E-04	0.238	730	1700
Mosc-17	1.36E-04	0.298	730	1700
Mosc-18	1.29E-04	0.353	730	1700
Mosc-21	1.04E-04	0.169	730	1700
Mosc-22	9.40E-05	0.147	730	1700
Mosc-23	1.06E-04	0.146	730	1700
Mosc-24	8.10E-05	0.166	730	1700
Mosc-25	1.27E-04	0.137	730	1700
Cop-1	1.40E-04	0.113	730	1700
Cop-2	1.32E-04	0.087	730	1700
Cop-3	1.15E-04	0.076	730	1700
Cop-4	1.21E-04	0.071	730	1700
Cop-5	7.50E-05	0.105	730	1700
Cop-6	1.27E-04	0.089	730	1700
Cop-7	1.70E-04	0.120	730	1700
Cop-8	1.55E-04	0.079	730	1700
Cop-9	8.90E-05	0.051	730	1700
Arist-S1	5.30E-05	0.032	730	1700
Arist-S2	8.20E-05	0.077	730	1700
Arsit-S3	5.90E-05	0.052	730	1700
Marius-1	4.10E-05	0.089	790	1700
Marius-2	4.80E-05	0.062	790	1700
Marius-3	4.60E-05	0.062	790	1700

[a]Slope value assumes band shifts are in units of nm, and local continuum slopes are in units of reflectance/nm.
[b]Tan stands for tangent.

nature of the 2 μm absorptions suggest that the Marius olivine spectra exhibit minor contamination from pyroxene, although the pyroxene composition is uncertain. Pyroxene contamination would also help to explain the relatively narrow 1000 nm absorption, as well as the short-wavelength band minimum. The spectral variability between Marius and the other spectra evaluated suggests a different composition or lithological association.

5.2.2. Quantitative Spectral Diversity

[29] The MGM fits quantify the spectral variability illustrated in Figure 9. The relative predicted olivine compositions derived from the deconvolutions to the Moscoviense and Copernicus spectra are presented in Figure 11. As expected based on their overall similarity in Figure 9, the Moscoviense and Copernicus olivines are predicted to be quite similar in composition, although the spectral variability of the Moscoviense spectra is manifested in the larger range in estimated relative composition (~30 relative Fo # units). The Copernicus deconvolutions appear to be balanced by competing influences: the apparently strong but narrow long-wavelength absorption and the sharp feature near ~850 nm. The Aristarchus and Marius spectra are clearly olivine-rich, but the contamination from other phases prevents us from using MGM fits to predict the olivines' compositions, as discussed in section 5.2.3.

[30] Figure 11 also illustrates the error brackets determined using the methods described above in section 3.3.2. The error brackets in effect indicate the range of results obtained from various fitting procedures applied to a single

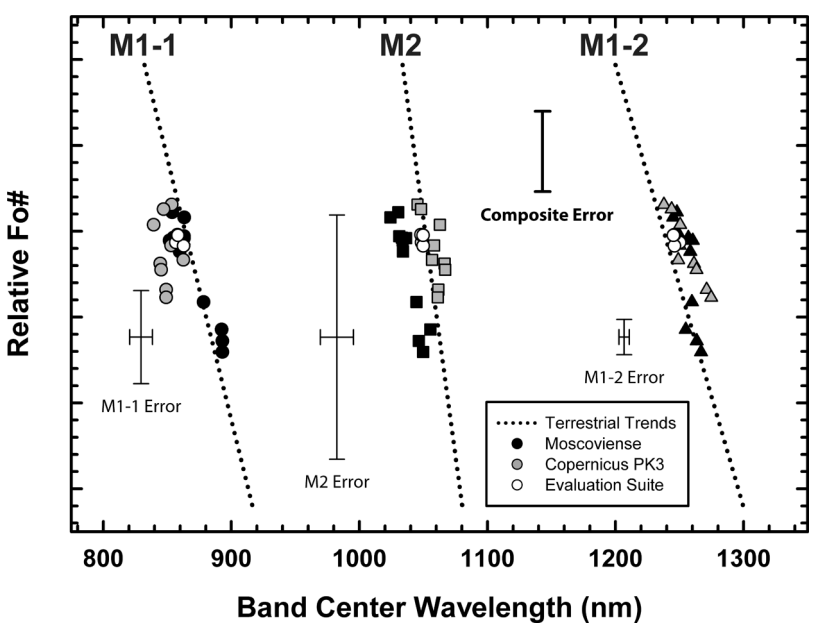

Figure 11. MGM-derived band center wavelengths and relative predicted compositions for the M^3 spectra analyzed in this study. The large ticks on the relatlive Fo # axis denote intervals of 20 relative Fo # units. The plotted results are reported in Table S1 in the auxiliary material. There is some deviation from the trends developed for terrestrial olivines by *Sunshine and Pieters* [1998], most notably for the central M2 absorption, but the overall agreement is reasonable. Error "range" brackets are reported for each component absorption (two-dimensional range) and for an overall range in predicted compositions. The composite error reflects the range in predicted composition when considering the ranges for each component absorption simultaneously. Error analysis is discussed more thoroughly in section 3.3.2.

M^3 spectrum. The error brackets (and the associated composite error bracket) do not evaluate the effect of each potential source of error (e.g., reduced spectral resolution, increased noise, etc.) explicitly, but do evaluate them in the sense that all sources of error contribute to the observed ranges. Future work on this subject will likely focus on deconvolutions of laboratory spectra with reduced spectral sampling and various levels of random noise introduced in order to quantify these effects more explicitly. Even in the ideal case of MGM deconvolutions of laboratory olivine reflectance spectra, compositional predictions with this approach can be accurate only to within ~5–10% (5–10 Fo # units) [*Sunshine and Pieters*, 1998; *Isaacson and Pieters*, 2010]. The range predicted for the "composite error" is on the order of 20 Fo # units (on a 0–100 scale in molar Mg/Mg +Fe *100). Thus, our reported compositions should be viewed and interpreted as approximate solutions, even in a relative sense.

[31] The relative olivine compositions predicted from the M^3 spectra can be used to draw some geological interpretations. The Moscoviense olivines appear to be diverse but Mg-rich relative to the other olivines evaluated here. The most Mg-rich compositions found at Moscoviense appear consistent with the evaluation suite results, which in absolute terms are similar to some of the most Mg-rich olivines found in Mg suite rocks with compositions near ~Fo_{90} [e.g., *Papike et al.*, 1998]. While there are reasons to be cautious in interpreting this similarity, it is suggestive that the olivines found to be the most Mg-rich in the region may be quite Mg-rich in absolute terms as well. This may suggest that these olivines are derived from a relatively primitive plutonic source, which would be consistent with the plutonism hypothesized to have produce the unusual mafic lithologies observed elsewhere in the Moscoviense region [*Pieters et al.*, 2011]. Our results do not allow us to evaluate a possible genetic relationship to the olivines studied at Moscoviense and those identified in association with unusual exposures of olivine, orthopyroxene, and spinel (OOS) by *Pieters et al.* [2011], largely because the olivines identified by Pieters *et al.* do not exhibit sufficient spectral contrast or purity to evaluate with our current approach. However, such a comparison would be a logical avenue for future work if the spectral contrast and purity issues can be overcome. The diversity of the olivine compositions observed at Moscoviense may indicate a long-lived geologic process capable of producing a trend in olivine compositions toward more Fe-rich compositions as the olivine's source material evolved. The observed diversity is distributed across a relatively small spatial region (less than 100 km^2), and a wide variation in olivine composition across a small area is difficult to explain petrologically. However, the large error bars in these analyses may help explain some of the widespread variation (the actual compositional diversity may be magnified by errors). Additionally, it is of course possible that random noise may contribute to the observed heterogeneity. However, the real spectral differences apparent in Figure 9 suggest that real compositional variability is largely responsible for the spread in predicted compositions. Regardless, the diverse compositions observed for the Moscoviense olivines suggest a different process than that responsible for the olivines at Copernicus, which are spectrally (and thus compositionally) more homogenous.

[32] The olivines at Copernicus are found to be relatively Mg-rich, comparable to the most Mg-rich of the compositions predicted at Moscoviense. Additionally, they are more spectrally and thus compositionally homogeneous than those observed at Moscoviense. Their predicted compositions are also similar to those of the evaluation suite spectra. The consistency between all spectra analyzed for the Copernicus central peak indicates that the olivine is fairly homogenous in composition, which is consistent with a single magmatic or mantle source, rather than a process in which a source region evolved over time producing a trend of increasing olivine Fe contents. The relatively Mg-rich compositions argue against a volcanic origin and in favor of a plutonic origin, as olivines in mare basalt largely (but not always) tend to be somewhat more Fe-rich [e.g., *Papike et al.*, 1976]. As the Aristarchus and Marius spectra exhibit clear contributions from absorptions not due to olivine, we elect not to model them with the MGM, as the results would be biased by the other absorptions in the general 1000 nm region where the principal olivine absorptions are found. We merely point out their clear spectral differences from the Moscoviense and Copernicus spectra, which alone are sufficient to demonstrate the different lithological associations of the Aristarchus and Marius olivines relative to those at Moscoviense and Copernicus.

5.2.3. Mixtures

[33] Currently, our approach is likely to produce meaningful results only for spectra in which olivine is the dominant phase (i.e., no other ferrous absorptions in the 1000 nm region). This rules out compositional analyses of pyroxene-olivine mixtures. Olivine-plagioclase mixtures can be analyzed, especially if the plagioclase is in its shocked form (maskelynite) and lacks its typical feature near 1300 nm [e.g., *Bell and Mao*, 1973; *Adams and Goullaud*, 1978; *Pieters*, 1996]. Crystalline, Fe-bearing plagioclase does exhibit absorptions near 1300 nm, and if such absorption features were detectible in the olivine-plagioclase mixture spectrum, that spectrum could not be analyzed with our present approach. However, the plagioclase absorption feature does tend to get masked by other mafic absorptions such as those of olivine and pyroxene [e.g., *Isaacson et al.*, 2011], meaning that olivine-plagioclase mixtures generally can be analyzed with our approach except in rare cases where the plagioclase absorption feature persists.

[34] In principle, our approach could be applied to spectra of mixtures such as olivine-pyroxene. The potential problems associated with extending the approach to mixture spectra lie in determining the properties of the olivine absorptions in the presence of additional absorptions near 1000 nm, as discussed above in the context of the Marius olivine spectra. The MGM seeks a mathematically optimized solution, without regard for whether or not the fit is physically reasonable (consistent with the mineralogy of the material represented by the input spectrum). Each Gaussian is based on three model parameters (position, strength, and width), so the presence of additional absorption features substantially increases the number of free parameters in the model, and reduces the likelihood of obtaining a unique and physically reasonable fit. *McFadden and Cline* [2005] used the MGM to model laboratory reflectance spectra of Martian meteorites, including several containing mixtures of olivine and pyroxene. While they were able to produce reasonable

fits in some cases, they were unable to produce acceptable fits for several other such mixtures, even in analyzing optimal quality laboratory spectra. The increased noise level and decreased spectral resolution of M^3 relative to laboratory spectra have been discussed above, and combine to make obtaining acceptable results for pyroxene/olivine mixtures extremely challenging with the current approach. However, if a method to constrain the model parameters appropriately and allow the olivine absorptions to be deconvolved properly were available, our approach could certainly be used to estimate the composition of the olivine. For example, the 2000 nm pyroxene absorption feature could be used to help constrain the Gaussian(s) used to model the pyroxene 1000 nm absorption feature, as the properties of the pyroxene absorption features are related [e.g., *Adams*, 1974; *Hazen et al.*, 1978; *Cloutis et al.*, 1986; *Klima*, 2008]. In the case of lunar olivine, however, this approach would in turn be complicated by the presence of the chromite absorptions near 2000 nm.

6. Conclusions

[35] Our analyses of olivines using Chandrayaan-1 Moon Mineralogy Mapper (M^3) spectra have produced intriguing results. Suites of olivine reflectance spectra collected from diverse regions on the lunar surface exhibit spectral variability through visual comparisons. The MGM was used to quantify these observations for the olivine-dominated spectra. Olivine from the Copernicus central peak was found to be fairly homogenous and, broadly speaking, compositionally similar to olivines from Moscoviense, though the Moscoviense olivines were found to be slightly more spectrally and thus compositionally diverse. While the cautions presented here must be considered carefully, the methods presented in this paper can be used to make general predictions of absolute olivine composition (Fe/Mg content) with remotely sensed VNIR reflectance spectra. While the error bars in our results are substantial given the numerous issues discussed here, our results suggest the detection of Mg-rich olivine at Moscoviense and Copernicus with M^3 spectra. Olivines from the Aristarchus crater were found to be exhibit a strong long-wavelength absorption, likely due to contamination by a presently unknown phase. The origin of this strong long-wavelength absorption is presently unclear, but it does suggest a compositional difference or at least a different lithological association than exhibited by the Moscoviense and Copernicus olivines. Olivines at Marius were found to exhibit contamination, likely by pyroxene, which again hints at a different lithological association than exhibited by the olivines at Copernicus and Moscoviense.

[36] The present study has demonstrated a systematic approach for addressing variable continuum slopes common to remotely sensed spectra of planetary surfaces, and discussed some of the strengths and weaknesses of this simplified but easily repeatable and consistent approach. Using a suite of laboratory spectra, we have demonstrated that our tangential continuum removal process is able to treat the effects of variable continuum slopes in a consistent manner. This is a vital step, as lack of such a treatment would lead to derived band positions (and thus predicted compositions) that are strongly biased by continuum slopes. The reduced spectral sampling and lower signal-to-noise ratio of the M^3 spectra relative to typical laboratory spectra affect the accuracy of compositional predictions. We have quantified the likely range in a predicted composition, but have not treated sources of error explicitly beyond their contribution to a bulk overall "error" in our relative compositional predictions. Future work on this topic will involve expanding the survey to analyze olivines from more regions on the lunar surface.

[37] **Acknowledgments.** The efforts of the entire M^3 engineering, operations, and science teams are gratefully acknowledged. M^3 science validation is supported through NASA contract NNM05AB26C. M^3 is supported as a NASA Discovery Program mission of opportunity. The M^3 team is grateful to ISRO for the opportunity to fly as a guest instrument on Chandrayaan-1. Partial funding for this analysis has also been provided through the NASA LSI at Brown University under contract NNA09DB34A. Careful reviews by Brett Denevi and an anonymous reviewer have improved this manuscript substantially. The views, opinions, and/or findings contained in this paper are those of the authors and should not be interpreted as representing the official views, either expressed or implied, of the Defense Advanced Research Projects Agency or the Department of Defense.

References

Adams, J. B. (1974), Visible and near-infrared diffuse reflectance spectra of pyroxenes as applied to remote sensing of solid objects in the solar system, *J. Geophys. Res.*, *79*, 4829–4836, doi:10.1029/JB079i032p04829.

Adams, J. B., and L. H. Goullaud (1978), Plagioclase feldspars: Visible and near infrared diffuse reflectance spectra as applied to remote sensing, *Proc. Lunar Planet Sci.*, *9*, 2901–2909.

Andersson, L. E., and E. A. Whitaker (1982), NASA Catalogue of Lunar Nomenclature, *NASA Ref. Publ., 1097*.

Aronson, J. R., L. H. Bellotti, S. W. Eckroad, R. K. McConnell, and P. C. Von Thüna (1970), Infrared spectra and radiative thermal conductivity of minerals at high temperatures, *J. Geophys. Res.*, *75*(17), 3443–3456, doi:10.1029/JB075i017p03443.

Basaltic Volcanism Study Project (BVSP) (1981), *Basaltic Volcanism on the Terrestrial Planets*, Pergamon, New York.

Bell, P. M., and H. K. Mao (1973), Optical and chemical analysis of iron in Luna 20 plagioclase, *Geochim. Cosmochim. Acta*, *37*, 755–759, doi:10.1016/0016-7037(73)90172-5.

Besse, S., J. M. Sunshine, M. I. Staid, N. E. Petro, J. W. Boardman, R. O. Green, J. W. Head, P. J. Isaacson, J. F. Mustard, and C. M. Pieters (2011), Compositional variability of the Marius Hills Volcanic Complex from the Moon Mineralogy Mapper (M^3), *J. Geophys. Res.*, doi:10.1029/2010JE003725, in press.

Boardman, J. W., C. M. Pieters, R. O. Green, S. Lundeen, P. Varansi, J. Nettles, N. E. Petro, P. J. Isaacson, S. Besse, and L. A. Taylor (2011), Measuring moonlight: An overview of the spatial properties, lunar coverage, selenolocation and related level 1B products of the Moon Mineralogy Mapper, *J. Geophys. Res.*, doi:10.1029/2010JE003730, in press.

Burns, R. G. (1970), Crystal field spectra and evidence of cation ordering in olivine minerals, *Am. Mineral.*, *55*, 1608–1632.

Burns, R. G. (1974), The polarized spectra of iron in silicates: Olivine. A discussion of neglected contributions from Fe^{2+} ions in M(1) sites, *Am. Mineral.*, *59*, 625–629.

Burns, R. G. (1993), *Mineralogical Applications of Crystal Field Theory*, 2nd ed., 551 pp., Cambridge Univ. Press, New York, doi:10.1017/CBO9780511524899.

Burns, R. G., F. E. Huggins, and R. M. Abu-Eid (1972), Polarized absorption spectra of single crystals of lunar pyroxenes and olivines, *Moon*, *4*, 93–102, doi:10.1007/BF00562917.

Chevrel, S. D., P. C. Pinet, Y. Daydou, S. Le Mouélic, Y. Langevin, F. Costard, and S. Erard (2009), The Aristarchus Plateau on the Moon: Mineralogical and structural study from integrated Clementine UV Vis NIR spectral data, *Icarus*, *199*, 9–24, doi:10.1016/j.icarus.2008.08.005.

Clark, R. N. (1999), Spectroscopy of rocks and minerals, and principles of spectroscopy, in *Manual of Remote Sensing*, vol. 3, *Remote Sensing for the Earth Sciences*, edited by A. N. Rencz, pp. 3–58, John Wiley, New York.

Clark, R. N., and T. L. Roush (1984), Reflectance spectroscopy: Quantitative analysis techniques for remote sensing applications, *J. Geophys. Res.*, *89*, 6329–6340, doi:10.1029/JB089iB07p06329.

Clark, R. N., C. M. Pieters, R. O. Green, J. W. Boardman, and N. E. Petro (2011), Thermal removal from near-infrared imaging spectroscopy data of the Moon, *J. Geophys. Res.*, doi:10.1029/2010JE003751, in press.

Cloutis, E. A., M. J. Gaffey, T. L. Jackowski, and K. L. Reed (1986), Calibrations of phase abundance, composition, and particle size distribution for olivine-orthopyroxene mixtures from reflectance spectra, *J. Geophys. Res.*, *91*, 11,641–11,653, doi:10.1029/JB091iB11p11641.

Cloutis, E. A., J. M. Sunshine, and R. V. Morris (2004), Spectral reflectance-compositional properties of spinels and chromites: Implications for planetary remote sensing and geothermometry, *Meteorit. Planet. Sci.*, *39*, 545–565, doi:10.1111/j.1945-5100.2004.tb00918.x.

Dyar, M. D., et al. (2009), Spectroscopic characteristics of synthetic olivine: An integrated multi-wavelength and multi-technique approach, *Am. Mineral.*, *94*(7), 883–898, doi:10.2138/am.2009.3115.

Hapke, B. (2001), Space weathering from Mercury to the asteroid belt, *J. Geophys. Res.*, *106*, 10,039–10,073, doi:10.1029/2000JE001338.

Hazen, R. M., P. M. Bell, and H. K. Mao (1978), Effects of compositional variation on absorption spectra of lunar pyroxenes, *Proc. Lunar Planet Sci.*, *9*, 2919–2934.

Hicks, M. D., B. J. Buratti, J. Nettles, M. Staid, J. Sunshine, C. M. Pieters, S. Besse, and J. W. Boardman (2011), A photometric function for analysis of lunar images in the visual and infrared based on Moon Mineralogy Mapper observations, *J. Geophys. Res.*, doi:10.1029/2010JE003733, in press.

Hiroi, T., and S. Sasaki (2001), Importance of space weathering simulation products in compositional modeling of asteroids: 349 Dembowska and 446 Aeternitas as examples, *Meteorit. Planet. Sci.*, *36*, 1587–1596, doi:10.1111/j.1945-5100.2001.tb01850.x.

Isaacson, P. J., and C. M. Pieters (2010), Deconvolution of lunar olivine reflectance spectra: Implications for remote compositional assessment, *Icarus*, *210*(1), 8–13, doi:10.1016/j.icarus.2010.06.004.

Isaacson, P. J., A. Basu Sarbadhikari, C. M. Pieters, R. L. Klima, T. Hiroi, Y. Liu, and L. A. Taylor (2011), The lunar rock and mineral characterization consortium: Deconstruction and integrated mineralogical, petrologic, and spectroscopic analyses of mare basalts, *Meteorit. Planet. Sci.*, *46*, 228–251, doi:10.1111/j.1945-5100.2010.01148.x.

Kanner, L. C., J. F. Mustard, and A. Gendrin (2007), Assessing the limits of the Modified Gaussian Model for remote spectroscopic studies of pyroxenes on Mars, *Icarus*, *187*, 442–456, doi:10.1016/j.icarus.2006.10.025.

King, T. V. V., and W. I. Ridley (1987), Relation of the spectroscopic reflectance of olivine to mineral chemistry and some remote sensing implications, *J. Geophys. Res.*, *92*, 11,457–11,469, doi:10.1029/JB092iB11p11457.

Klima, R. L. (2008), Integrated spectroscopy of synthetic Mg-Fe-Ca pyroxenes, Ph.D. thesis, 281 pp., Brown Univ., Providence, R. I.

Le Mouélic, S. (2001), The olivine at the lunar crater Copernicus as seen by Clementine NIR data, *Planet. Space Sci.*, *49*, 65–70, doi:10.1016/S0032-0633(00)00091-X.

Le Mouélic, S., Y. Langevin, and S. Erard (1999a), The distribution of olivine in the crater Aristarchus inferred from Clementine NIR data, *Geophys. Res. Lett.*, *26*, 1195–1198, doi:10.1029/1999GL900180.

Le Mouélic, S., Y. Langevin, and S. Erard (1999b), A new data reduction approach for the Clementine NIR data set: Application to Aristillus, Aristarchus and Kepler, *J. Geophys. Res.*, *104*, 3833–3843, doi:10.1029/1998JE900035.

Lucey, P. G. (1998), Model near-infrared optical constants of olivine and pyroxene as a function of iron content, *J. Geophys. Res.*, *103*, 1703–1713, doi:10.1029/97JE03145.

Lucey, P. G., B. R. Hawke, and K. Horton (1991), The distribution of olivine in the Crater Copernicus, *Geophys. Res. Lett.*, *18*(11), 2133–2136, doi:10.1029/91GL02538.

McFadden, L. A., and T. P. Cline (2005), Spectral reflectance of Martian meteorites: Spectral signatures as a template for locating source region on Mars, *Meteorit. Planet. Sci.*, *40*, 151–172, doi:10.1111/j.1945-5100.2005.tb00372.x.

Mustard, J. F., et al. (2011), Compositional diversity and geologic insights of the Aristarchus crater from Moon Mineralogy Mapper data, *J. Geophys. Res.*, doi:10.1029/2010JE003726, in press.

Noble, S. K., C. M. Pieters, L. A. Taylor, R. V. Morris, C. C. Allen, D. S. McKay, and L. P. Keller (2001), The optical properties of the finest fraction of lunar soil: Implications for space weathering, *Meteorit. Planet. Sci.*, *36*, 31–42, doi:10.1111/j.1945-5100.2001.tb01808.x.

Noble, S. K., L. P. Keller, and C. M. Pieters (2005), Evidence of space weathering in regolith breccias I: Lunar regolith breccias, *Meteorit. Planet. Sci.*, *40*, 397–408, doi:10.1111/j.1945-5100.2005.tb00390.x.

Noble, S. K., C. M. Pieters, and L. P. Keller (2007), An experimental approach to understanding the optical effects of space weathering, *Icarus*, *192*(2), 629–642, doi:10.1016/j.icarus.2007.07.021.

Ohtake, M., et al. (2009), The global distribution of pure anorthosite on the Moon, *Nature*, *461*(7261), 236–240, doi:10.1038/nature08317.

Papike, J. J., F. N. Hodges, A. E. Bence, M. Cameron, and J. M. Rhodes (1976), Mare basalts: Crystal chemistry, mineralogy, and petrology, *Rev. Geophys. Space Phys.*, *14*, 475–540, doi:10.1029/RG014i004p00475.

Papike, J. J., G. Ryder, and C. K. Shearer (1998), Lunar samples, in *Planetary Materials*, edited by J. J. Papike, pp. 5-1–5-234, Mineral. Soc. of Am., Washington, D. C.

Pieters, C. M. (1982), Copernicus crater central peak: Lunar mountain of unique composition, *Science*, *215*, 59–61, doi:10.1126/science.215.4528.59.

Pieters, C. M. (1986), Composition of the lunar highland crust from near-infrared spectroscopy, *Rev. Geophys. Space Phys.*, *24*(3), 557–578, doi:10.1029/RG024i003p00557.

Pieters, C. M. (1996), Plagioclase and maskelynite diagnostic features, *Lunar Planet. Sci. [CD-ROM]*, *27*, 1031.

Pieters, C. M. (1999), The moon as a spectral calibration standard enabled by lunar samples: The Clementine example, paper presented at Workshop on New Views of the Moon II: Understanding the Moon Through the Integration of Diverse Datasets, Lunar and Planet. Inst., Flagstaff, Ariz.

Pieters, C. M., and D. E. Wilhelms (1985), Origin of olivine at Copernicus, *Proc. Lunar Planet. Sci.*, *15*, 415–420.

Pieters, C. M., L. A. Taylor, S. K. Noble, L. P. Keller, B. Hapke, R. V. Morris, C. C. Allen, D. S. McKay, and S. Wentworth (2000), Space weathering on airless bodies: Resolving a mystery with lunar samples, *Meteorit. Planet. Sci.*, *35*, 1101–1107, doi:10.1111/j.1945-5100.2000.tb01496.x.

Pieters, C. M., et al. (2009), The Moon Mineralogy Mapper (M^3) on Chandrayaan-1, *Curr. Sci.*, *96*(4), 500–505.

Pieters, C. M., et al. (2011), Mg-spinel lithology: A new rock-type on the lunar farside, *J. Geophys. Res.*, doi:10.1029/2010JE003727, in press.

Sasaki, S., T. Hiroi, K. Nakamura, Y. Hamabe, E. Kurahashi, and M. Yamada (2002), Simulation of space weathering by nanosecond pulse laser heating: Dependence on mineral composition, weathering trend of asteroids and discovery of nanophase iron particles, *Adv. Space Res.*, *29*(5), 783–788, doi:10.1016/S0273-1177(02)00012-1.

Sasaki, S., E. Kurahashi, C. Yamanaka, and K. Nakamura (2003), Laboratory simulation of space weathering: Changes of optical properties and TEM/ESR confirmation of nanophase metallic iron, *Adv. Space Res.*, *31*(12), 2537–2542, doi:10.1016/S0273-1177(03)00575-1.

Singer, R. B., and T. L. Roush (1985), Effects of temperature on remotely sensed mineral absorption features, *J. Geophys. Res.*, *90*, 12,434–12,444, doi:10.1029/JB090iB14p12434.

Sunshine, J. M., and C. M. Pieters (1998), Determining the composition of olivine from reflectance spectroscopy, *J. Geophys. Res.*, *103*, 13,675–13,688, doi:10.1029/98JE01217.

Sunshine, J. M., C. M. Pieters, and S. F. Pratt (1990), Deconvolution of mineral absorption bands: An improved approach, *J. Geophys. Res.*, *95*, 6955–6966, doi:10.1029/JB095iB05p06955.

Sunshine, J. M., S. J. Bus, C. M. Corrigan, T. J. McCoy, and T. H. Burbine (2007), Olivine-dominated asteroids and meteorites: Distinguishing nebular and igneous histories, *Meteorit. Planet. Sci.*, *42*(2), 155–170, doi:10.1111/j.1945-5100.2007.tb00224.x.

Taylor, L. A., C. M. Pieters, L. P. Keller, R. V. Morris, and D. S. McKay (2001), Lunar mare soils: Space weathering and the major effects of surface-correlated nanophase Fe, *J. Geophys. Res.*, *106*, 27,985–27,999, doi:10.1029/2000JE001402.

Taylor, L. A., C. Pieters, A. Patchen, D.-H. S. Taylor, R. V. Morris, L. P. Keller, and D. S. McKay (2010), Mineralogical and chemical characterization of lunar highland soils: Insights into the space weathering of soils on airless bodies, *J. Geophys. Res.*, *115*, E02002, doi:10.1029/2009JE003427.

Yamada, M., S. Sasaki, H. Nagahara, A. Fujiwara, S. Hasegawa, H. Yano, T. Hiroi, H. Ohashi, and H. Otake (1999), Simulation of space weathering of planet-forming materials: Nanosecond pulse laser irradiation and proton implantation on olivine and pyroxene samples, *Earth Planets Space*, *51*, 1255–1265.

Yamamoto, S., et al. (2010), Possible mantle origin of olivine around lunar impact basins detected by SELENE, *Nat. Geosci.*, *3*, 533–536, doi:10.1038/ngeo897.

S. Besse and J. M. Sunshine, Department of Astronomy, University of Maryland, College Park, MD 20742-2421, USA.

R. N. Clark, U.S. Geological Survey, MS964, Box 25046, Federal Center, Denver, CO 80225, USA.

J. W. Head, P. J. Isaacson, J. F. Mustard, and C. M. Pieters, Department of Geological Sciences, Brown University, Box 1846, Providence, RI 02912, USA. (Peter_Isaacson@Brown.edu)

R. L. Klima, Johns Hopkins University Applied Physics Laboratory, 11100 Johns Hopkins Rd., Laurel, MD 20732-0000, USA.
N. E. Petro, NASA Goddard Space Flight Center, Code 698, Greenbelt, MD 20771, USA.
M. I. Staid, Planetary Science Institute, 1700 E. Fort Lowell, Ste. 106, Tucson, AZ 85719, USA.
L. A. Taylor and K. G. Thaisen, Planetary Geosciences Institute, Department of Earth and Planetary Sciences, University of Tennessee, 1412 Circle Dr., Knoxville, TN 37996-1410, USA.
S. Tompkins, Defense Advanced Research Projects Agency, 3701 N. Fairfax Dr., Arlington, VA 22203-1714, USA.